

On the topographic Rossby solitary waves via physical-informed neural networks

Wenxu Liu(刘文绪), Ligeyan Dao(道力格艳), and Ruigang Zhang(张瑞岗)
Citation: Chin. Phys. B, 2025, 34 (**7**): 070504. DOI: 10.1088/1674-1056/adc7f1
Journal homepage: http://cpb.iphy.ac.cn; http://iopscience.iop.org/cpb

What follows is a list of articles you may be interested in

Abundant invariant solutions of (3+1)-dimensional combined pKP-BKP equation

Hengchun Hu(胡恒春) and Xu Xu(徐旭)
Chin. Phys. B, 2025, 34 (**3**): 030501. DOI: 10.1088/1674-1056/ada43b

The *N*-periodic wave solutions to the *N* =1 supersymmetric Sawada-Kotera-Ramani equation

Pengcheng Xin(辛鹏程), Zhonglong Zhao(赵忠龙), and Yu Wang(王宇)
Chin. Phys. B, 2025, 34 (**2**): 020502. DOI: 10.1088/1674-1056/ad9912

Excitation threshold of solitons in anharmonic chains

Yi Ming(明燚)
Chin. Phys. B, 2025, 34 (**2**): 020501. DOI: 10.1088/1674-1056/ad9ff6

Localized wave solutions and interactions of the (2+1)-dimensional Hirota—Satsuma—Ito equation

Qiankun Gong(巩乾坤), Hui Wang(王惠), and Yunhu Wang(王云虎)
Chin. Phys. B, 2024, 33 (**4**): 040505. DOI: 10.1088/1674-1056/ad1f4c

Compression and stretching of ring vortex in a bulk nonlinear medium

Xian-Jing Lai(来娴静), Xiao-Ou Cai(蔡晓鸥), Ya-Bin Shao(邵雅斌), and Yue-Yue Wang(王悦悦)
Chin. Phys. B, 2024, 33 (**2**): 020506. DOI: 10.1088/1674-1056/ad01a0

On the topographic Rossby solitary waves via physical-informed neural networks

Wenxu Liu(刘文绪), Ligeyan Dao(道力格艳), and Ruigang Zhang(张瑞岗)†

School of Mathematical Sciences, Inner Mongolia University, Hohhot 010021, *China*

(Received 2 February 2025; revised manuscript received 26 March 2025; accepted manuscript online 2 April 2025)

In the generation and propagation of nonlinear Rossby solitary waves within the atmosphere and ocean, topography occupies a pivotal role. This paper focuses on elucidating the impact of topography on such Rossby solitary waves. Utilizing the perturbation expansion method and spatialtemporal transformations, we derive the Korteweg–de Vries and modified Korteweg–de Vries equation (Gardner equation) governing the amplitude of nonlinear Rossby waves. A fundamental issue addressed herein is a Sturm–Liouville-type ordinary differential equation characterized by variable coefficients and fixed boundary conditions. To numerically solve the derived Korteweg–de Vries and modified Korteweg–de Vries equations, we employ a physical-informed neural network. Both qualitative and quantitative analyses are conducted to discuss the influences of topography and β effects, respectively.

Keywords: Rossby solitary wave, shallow water models, topography, physical-informed neural network

PACS: 05.45.Yv, 02.30.Mv, 47.11.St, 92.10.hf

DOI: 10.1088/1674-1056/adc7f1 **CSTR:** 32038.14.CPB.adc7f1

1. Introduction

Rossby wave[1] is a type of fluctuations in geophysical hydrodynamics that portray large-scale slow motions, which explain well not only the motions of ridges and troughs on high-altitude weather maps, but also weather changes near the ground. Many scholars have explained in detail the theories related to Rossby solitary waves in earlier studies, especially, on the development of solitary wave theory. Long[2] proved that the Rossby wave amplitude satisfies the Korteweg–de Vries (KdV) equation under the β-plane approximation. In addition, Wadati[3] derived the modified Korteweg–de Vries (mKdV) equation as an alternative model to describe nonlinear Rossby wave dynamics. Compared to the KdV equation, mKdV has stronger nonlinearity, which means it is preferentially applicable to motions with stronger perturbations. Luo[4] obtained the nonlinear Schrödinger (NLS) equation satisfied by the evolution of nonlinear Rossby wave packets, which suggests that the NLS equation is also a suitable model for describing nonlinear Rossby waves. Since then, more models used to describe Rossby waves, including the Benjamin–Ono (BO) equation,[5] the Zakharov–Kuznetsov (ZK) equation,[6] the Kadomtsev–Petviashvili (KP) equation,[7] etc., have been progressively developed. Recently, Hou *et al.*[8] isolated for the first time the quartic Korteweg–de Vries (quartic KdV) equation describing the amplitude of Rossby waves from the quasi-geostrophic potential vorticity and utilized it to discuss the nonlinearity of the physical mechanism of Rossby wave generation. Yang *et al.*[9] derived the (2+1)-dimensional coupled nonlinear Schrödinger (CNLS) equations that can describe interactions of two Rossby waves propagating in stratified fluids.

In real atmospheric and oceanic environments, many physical factors have a significant effect on nonlinear Rossby wave propagation, such as the β effect, the basic flow, topography, and dissipation. Hodyss *et al.*[10–13] considered the problem of the evolution of Rossby waves under the action of zonally varying flows and showed that latitudinal shear currents have a significant effect on both the phase velocity and amplitude of the wave amplitude. After Charney proposed the multiple flow equilibria theory,[14,15] the role of topography on Rossby waves gradually received attention from scholars. Yang *et al.* studied the effect of three different topographies, namely, linear topography,[16] slowly varying topography,[17] and spatialtemporal varying topography,[18] on Rossby waves. Han *et al.*[19] obtained the Benjamin–Ono equation from a barometric quasi-geostrophic model and found that large-scale topography-induced algebraic solitary waves do exist. Zhang *et al.*[20] employed the derivative expansion method to derive a nonlinear Schrödinger equation, demonstrating that topography exerts a notable influence on both the amplitude magnitude and propagation velocity of Rossby waves. Furthermore, the β effect is equally crucial in the generation and propagation of Rossby waves. Song *et al.*[21] derived the mKdV equation, which characterizes the evolution of the amplitude of Rossby solitary waves, and analyzed the impacts of the β effect, buoyancy frequency, and basic shear flow on these waves. Zhao *et al.*[22] discussed the Schrödinger equation satisfied by Rossby wave packets under the β effect.

Solving the partial differential equations (PDEs) remains

†Corresponding author. E-mail: rgzhang@imu.edu.cn

© 2025 Chinese Physical Society and IOP Publishing Ltd. All rights, including for text and data mining, AI training, and similar technologies, are reserved.

both an intriguing task and a challenging task. Over the past few decades, numerous analytical methods have been proposed, including the Hirota bilinear method,[23] the Jacobi elliptic function expansion method,[24] and the Bäcklund transform,[25] among others. Additionally, various numerical methods have proven to be powerful tools for addressing nonlinear equations, such as the finite difference method,[26] Fourier spectral method,[27] and lattice Boltzmann method.[28] In recent years, advancements in high-performance computing devices, particularly graphics processing units (GPUs), have facilitated the application of deep learning methods for solving PDEs. Notably, techniques such as physics-informed neural networks (PINN),[29] deep operator network (DeepONet),[30] and Fourier neural operators (FNO)[31] have emerged as promising alternatives for tackling these equations.

In recent years, utilizing deep learning methods for fluid dynamics modeling has emerged as a new direction in the field of scientific machine learning (SciML). Traditional fluid dynamics simulation methods often encounter challenges such as high computational costs and limited accuracy when dealing with highly complex and nonlinear problems. However, deep learning, with its powerful data processing and pattern recognition capabilities, offers a new solution for fluid dynamics research. The main applications of deep learning in fluid mechanics include: flow field modeling,[32,33] turbulence simulation,[34] and multiphase flow modeling.[35] In addition, we note that Shu *et al.*[36] have achieved the prediction of global extreme marine heatwaves (MHWs) using a physics-guided data-driven approach and Li *et al.*[37] analyzed the formation mechanism and dynamic behavior of the distorted waveform, which demonstrate that deep learning methods can also be applied in the fields of atmospheric and oceanic physics.

In this paper, we aim to explore the physical mechanism of nonlinear Rossby waves from a data-driven perspective through the introduction of the physics-informed neural network (PINN). The structure of this paper is as follows. In Section 2, we derive the KdV–mKdV equation, which describes the nonlinear Rossby wave amplitude under the influence of topography, from the original shallow water model equation. In Section 3, we solve the KdV–mKdV equation using a physics-informed neural network approach. This section also presents a qualitative and quantitative analysis of the impact of topography on the propagation of Rossby solitary waves, along with a discussion on the influence of the Rossby parameter β on these waves. In Section 4, some conclusions about the KdV–mKdV equation are summarized.

2. Derivation of nonlinear evolution equation

2.1. Basic model equations

Given that large-scale motions in the atmosphere and ocean can persist for days or longer, viscous effects are typically neglected. The shallow water model is usually adopted to be the basic model

$$\begin{cases} \dfrac{\partial u_*}{\partial t_*}+u_*\dfrac{\partial u_*}{\partial x_*}+u_*\dfrac{\partial u_*}{\partial y_*}-(f_0+\beta y_*)u_*=-g\dfrac{\partial \eta_*}{\partial x_*}, \\ \dfrac{\partial \upsilon_*}{\partial t_*}+u_*\dfrac{\partial \upsilon_*}{\partial x_*}+u_*\dfrac{\partial \upsilon_*}{\partial y_*}+(f_0+\beta y_*)u_*=-g\dfrac{\partial \eta_*}{\partial y_*}, \\ \dfrac{\partial \eta_*}{\partial t_*}+\dfrac{\partial}{\partial x_*}[u_*(H_*+\eta_*)]+\dfrac{\partial}{\partial y_*}[\upsilon_*(H_*+\eta_*)]=0, \end{cases} \tag{1}$$

where u_*, v_*, η_*, H_*, t_*, x_*, and y_* represent longitudinal and latitudinal velocities, surface fluctuations, undisturbed wave height, time, local east-westward coordinate, and north-southward coordinate, respectively. $f=f_0+\beta y_*$ is the Coriolis parameter, g denotes the acceleration of gravity.

The relative vorticity ξ_* is defined as

$$\xi_*=\frac{\partial \upsilon_*}{\partial x_*}-\frac{\partial u_*}{\partial y_*}. \tag{2}$$

The system of Eq. (1) can be reduced to the following potential vorticity conservation equation:

$$\frac{D}{Dt_*}\left(\frac{\xi_*+f}{H_*+\eta_*}\right)=0, \tag{3}$$

where

$$\frac{D}{Dt_*}=\frac{\partial}{\partial t_*}+u_*\frac{\partial}{\partial x_*}+v_*\frac{\partial}{\partial y_*}$$

is the material derivative. In order to consider the effect of topography on the propagation of nonlinear Rossby waves, we introduce the following stream function ψ_* based on the continuity equation with a rigid top boundary condition

$$\frac{\partial \psi_*}{\partial x_*}=H_*v_*,\quad \frac{\partial \psi_*}{\partial y_*}=-H_*u_*. \tag{4}$$

Then, the relative vorticity can be expressed as

$$\xi_*=\frac{1}{H_*}{\nabla_*}^2\psi_*-\frac{1}{{H_*}^2}\nabla_*\psi_*\cdot\nabla_*H_*, \tag{5}$$

where $\nabla_*=(\frac{\partial}{\partial x_*},\frac{\partial}{\partial y_*})$ represents the gradient operator. The first term of Eq. (5) represents the vorticity of the vertical water column and the second term represents the topographic vorticity. Substitution of Eq. (5) into Eq. (3) results in

$$\begin{aligned} &\frac{\partial}{\partial t_*}{\nabla_*}^2\psi_*-\frac{1}{H_*}\frac{\partial}{\partial t_*}\nabla_*\psi_*\cdot\nabla_*H_*+\frac{1}{H_*}J(\psi_*,{\nabla_*}^2\psi_*) \\ &-2\frac{{\nabla_*}^2\psi_*}{{H_*}^2}J(\psi_*,H_*)-\frac{\beta y_*}{H_*}J(\psi_*,H_*) \\ &+3\frac{\nabla_*\psi_*\cdot\nabla_*H_*}{{H_*}^3}J(\psi_*,H_*)-\frac{1}{{H_*}^2}J(\psi_*,\nabla_*\psi_*\cdot\nabla_*H_*) \\ &+H_*J\left(\psi_*,\frac{f_0}{H_*}\right)+\beta\frac{\partial \psi_*}{\partial x_*}=0. \end{aligned} \tag{6}$$

To further understand the mechanism of nonlinear Rossby waves, it is necessary to introduce some dimensionless quantities

$$(x_*, y_*) = L(x,y), \quad t_* = Tt, \quad u_* = Uu,$$
$$\psi_* = H_0 UL\psi, \quad H_* = H_0 H = H_0(1-\delta\eta_{\rm B}), \tag{7}$$

where L, H_0, T, U represents the horizontal length scale, the vertical length scale describing the depth variation, the spatial scale, and the velocity scale, respectively. $\eta_{\rm B}$ represents the non-dimensional seafloor topography.

Equation (8) is derived by substituting Eq. (7) into Eq. (6)

$$\begin{aligned}
&\omega\frac{\partial}{\partial t}\nabla^2\psi + \frac{\delta\omega}{1-\delta\eta_{\rm B}}\frac{\partial}{\partial t}\nabla\psi\cdot\nabla\eta_{\rm B} + \frac{R_0}{1-\delta\eta_{\rm B}}J(\psi,\nabla^2\psi)\\
&+\frac{\delta}{1-\delta\eta_{\rm B}}J(\psi,\eta_{\rm B}) + \frac{\delta R_0}{(1-\delta\eta_{\rm B})^2}J(\psi,\nabla\psi\cdot\nabla\eta_{\rm B})\\
&+\hat{\beta}\frac{\partial\psi}{\partial x} + 2\frac{\delta R_0\nabla^2\psi}{(1-\delta\eta_{\rm B})^2}J(\psi,\eta_{\rm B})\\
&+3\frac{\delta^2 R_0\nabla\psi\cdot\nabla\eta_{\rm B}}{(1-\delta\eta_{\rm B})^3}J(\psi,\eta_{\rm B}) + \frac{\delta\hat{\beta}y}{1-\delta\eta_{\rm B}}J(\psi,\eta_{\rm B}) = 0,
\end{aligned} \tag{8}$$

where $\omega = 1/f_0T$, $\delta = |(\partial H/\partial y)L|/H_0$ represents the aspect ratio, usually no more than 0.4, $R_0 = U/f_0L$ represents the Rossby number, which describes the importance of the Earth's rotation to the atmosphere and oceans. $\hat{\beta} = \beta L/f_0$ represents the non-dimensional beta.

To comprehend the physical mechanisms underlying nonlinear Rossby waves, certain assumptions or analyses are essential. We adopt the following assumptions $\hat{\beta}/\delta = \tilde{\beta}\delta$, $\omega \sim \delta \sim R_0/\delta$, $\delta/(1-\delta\eta_{\rm B}) \sim \delta$ and topographic change is influenced by longitude only, i.e., $\eta_{\rm B} = \eta_{\rm B}(y)$. Therefore, equation (8) can be further written as

$$\begin{aligned}
&\frac{\partial}{\partial t}\nabla^2\psi + \delta\frac{\partial}{\partial t}\left(\frac{\partial\psi}{\partial y}\eta'_{\rm B}\right) + (1+\delta\eta_{\rm B})\frac{\partial\psi}{\partial x}\eta'_{\rm B}\\
&+\delta J(\psi,\nabla^2\psi) + \tilde{\beta}\delta\frac{\partial\psi}{\partial x} + 2\delta^2\nabla^2\psi\frac{\partial\psi}{\partial x}\eta'_{\rm B}\\
&+\delta^2 J(\psi,\nabla\psi\cdot\nabla\eta_{\rm B}) + 3\delta^3\frac{\partial\psi}{\partial y}\eta'_{\rm B}\cdot\frac{\partial\psi}{\partial x}\eta'_{\rm B}\\
&+\tilde{\beta}\delta^2 y(1+\delta\eta_{\rm B})\frac{\partial\psi}{\partial x}\eta'_{\rm B} = 0,
\end{aligned} \tag{9}$$

where $\eta'_{\rm B}$ is the derivative of $\eta_{\rm B}$ with respect to y.

2.2. KdV–mKdV evolution equation for nonlinear Rossby waves

Due to the spatial and temporal multiscale nature of atmospheric and oceanic motions, introducing the Gardner–Morikawa transform to the variables x,t as

$$X = \delta(x-ct), \quad T = \delta^3 t, \tag{10}$$

where c is the wave speed, equation (9) then becomes

$$\begin{aligned}
&\left(\delta^3\frac{\partial}{\partial T} - c\delta\frac{\partial}{\partial X}\right)\left(\delta^2\frac{\partial^2\psi}{\partial X^2} + \frac{\partial^2\psi}{\partial y^2}\right)\\
&+\delta\eta'_{\rm B}\left(\delta^3\frac{\partial}{\partial T} - c\delta\frac{\partial}{\partial X}\right)\frac{\partial\psi}{\partial y} + \delta(1+\delta\eta_{\rm B})\eta'_{\rm B}\frac{\partial\psi}{\partial X}\\
&+\delta^2\frac{\partial\psi}{\partial X}\frac{\partial}{\partial y}\left(\delta^2\frac{\partial^2\psi}{\partial X^2} + \frac{\partial^2\psi}{\partial y^2}\right) + \tilde{\beta}y\delta^3\eta'_{\rm B}\frac{\partial\psi}{\partial X}\\
&-\delta^2\frac{\partial\psi}{\partial y}\frac{\partial}{\partial X}\left(\delta^2\frac{\partial^2\psi}{\partial X^2} + \frac{\partial^2\psi}{\partial y^2}\right) + \tilde{\beta}\delta^2\frac{\partial\psi}{\partial X}\\
&+\delta^3\frac{\partial\psi}{\partial X}\frac{\partial}{\partial y}\left(\eta'_{\rm B}\frac{\partial\psi}{\partial y}\right) + 2\delta^3\eta'_{\rm B}\left(\delta^2\frac{\partial^2\psi}{\partial X^2} + \frac{\partial^2\psi}{\partial y^2}\right)\frac{\partial\psi}{\partial X}\\
&+3\delta^4(\eta'_{\rm B})^2\frac{\partial\psi}{\partial y}\frac{\partial\psi}{\partial X} = 0.
\end{aligned} \tag{11}$$

Due to the nonlinearity of the considered problem, small parameter expansion of the stream function ψ is introduced as

$$\psi = \psi_0 + \delta\psi_1 + \delta^2\psi_2 + \cdots. \tag{12}$$

Substituting Eq. (12) into Eq. (11) leads to the following regimes for each order of the regression problem. For $o(\delta^1)$, we have

$$-c\frac{\partial}{\partial X}\left(\frac{\partial^2\psi_0}{\partial y^2}\right) + \eta'_{\rm B}\frac{\partial\psi_0}{\partial X} = 0. \tag{13}$$

Suppose that equation (13) has a separable variable solution of the following form:

$$\psi_0 = A(X,T)\phi_0(y), \tag{14}$$

and it leads to

$$\phi''_0(y) - \frac{\eta'_{\rm B}}{c}\phi_0(y) = 0. \tag{15}$$

Note that equation (15) with boundary conditions $\psi_0(-1) = \psi_0(1) = 0$ is an eigenvalue problem. Such problems can only determine the radial structure of the Rossby wave amplitude but not its evolution over space and time. Consequently, it is necessary to consider higher-order problems to fully understand the dynamics of the Rossby wave amplitude. For $o(\delta^2)$, we obtain

$$\begin{aligned}
&-c\frac{\partial}{\partial X}\frac{\partial^2\psi_1}{\partial y^2} + \eta'_{\rm B}\frac{\partial\psi_1}{\partial X}\\
&= c\eta'_{\rm B}\frac{\partial}{\partial X}\frac{\partial\psi_0}{\partial y} - \eta_{\rm B}\eta'_{\rm B}\frac{\partial\psi_0}{\partial X} - \frac{\partial\psi_0}{\partial X}\frac{\partial^3\psi_0}{\partial y^3}\\
&+\frac{\partial\psi_0}{\partial y}\frac{\partial}{\partial X}\frac{\partial^2\psi_0}{\partial y^2} - \tilde{\beta}\frac{\partial\psi_0}{\partial X}.
\end{aligned} \tag{16}$$

Suppose that equation (16) has a separable variable solution of the following form:

$$\psi_1 = B_1(X,T)\phi_1(y) + B_2(X,T)\phi_2(y). \tag{17}$$

Substituting Eq. (17) into Eq. (16). Without loss of generality, we assume $B_1 = A$, $B_2 = \frac{1}{2}A^2$, equation (16) can be written as

$$\phi''_1(y) - \frac{\eta'_{\rm B}}{c}\phi_1(y) = \frac{\eta_{\rm B}\eta'_{\rm B} + \tilde{\beta}}{c}\phi_0(y) - \eta'_{\rm B}\phi'_0(y), \tag{18}$$

$$\phi_2''(y)-\frac{\eta_B'}{c}\phi_2(y)=\frac{1}{c}(\phi_0(y)\phi_0'''(y)-\phi_0'(y)\phi_0''(y)). \quad (19)$$

Equations (18) and (19) with boundary conditions $\psi_i(-1)=\psi_i(1)=0$ $(i=1,2)$ are also an eigenvalue problem and do not determine the Rossby wave amplitude $A(X,T)$. So we move on to higher order problems. For $o(\delta^3)$, we have

$$-c\frac{\partial}{\partial X}\frac{\partial^2\psi_2}{\partial y^2}+\eta_B'\frac{\partial\psi_2}{\partial X}=F, \quad (20)$$

with

$$\begin{aligned}F=&-\frac{\partial}{\partial T}\frac{\partial^2\psi_0}{\partial y^2}+c\frac{\partial^3\psi_0}{\partial X^3}-\eta_B''\frac{\partial\psi_0}{\partial X}\frac{\partial\psi_0}{\partial y}-2\eta_B'\frac{\partial\psi_0}{\partial X}\frac{\partial^2\psi_0}{\partial y^2}\\&-\tilde{\beta}y\eta_B'\frac{\partial\psi_0}{\partial X}+c\eta_B'\frac{\partial}{\partial X}\frac{\partial\psi_1}{\partial y}-\eta_B\eta_B'\frac{\partial\psi_1}{\partial X}-\frac{\partial\psi_1}{\partial X}\frac{\partial^3\psi_0}{\partial y^3}\\&-\frac{\partial\psi_0}{\partial X}\frac{\partial^3\psi_1}{\partial y^3}+\frac{\partial\psi_1}{\partial y}\frac{\partial}{\partial X}\frac{\partial^2\psi_0}{\partial y^2}\\&+\frac{\partial\psi_0}{\partial y}\frac{\partial}{\partial X}\frac{\partial^2\psi_1}{\partial y^2}-\tilde{\beta}\frac{\partial\psi_1}{\partial X}. \quad (21)\end{aligned}$$

It can be seen that equations (20) and (13) have the same homogeneous part, so the necessary conditions must be satisfied

$$\int_0^1 F\phi_0(y)\mathrm{d}y=0. \quad (22)$$

After substituting Eqs. (14), (15), (17), (18), and (19) into Eq. (22), the resulting model equation is as follows:

$$\frac{\partial A}{\partial T}+I_1\frac{\partial A}{\partial X}+I_2A\frac{\partial A}{\partial X}+I_3A^2\frac{\partial A}{\partial X}+I_4\frac{\partial^3A}{\partial X^3}=0, \quad (23)$$

where

$$\begin{aligned}I=&-\int_0^1\eta_B'(y)\phi_0^2(y)\mathrm{d}y,\\I_1=&\frac{1}{I}\Big[-c\tilde{\beta}\int_0^1 y\eta_B'(y)+c^2\int_0^1\eta_B'(y)\phi_1'(y)\phi_0(y)\\&-c\int_0^1\eta_B(y)\eta_B'(y)\phi_1(y)\phi_0(y)\mathrm{d}y\\&-c\tilde{\beta}\int_0^1\phi_1(y)\phi_0(y)\mathrm{d}y\Big],\\I_2=&\frac{1}{I}\Big\{-3\int_0^1[\eta_B'(y)]^2\phi_0^3(y)\mathrm{d}y\\&+c^2\int_0^1\eta_B'(y)\phi_2'(y)\phi_0(y)\mathrm{d}y+c\int_0^1\phi_2(y)\phi_0(y)\mathrm{d}y\\&-c\int_0^1\eta_B(y)\eta_B'(y)\phi_2(y)\phi_0(y)\mathrm{d}y\\&-2\int_0^1\eta_B''(y)\phi_1(y)\phi_0^2(y)+\int_0^1\eta_B'(y)\phi_1'(y)\phi_0^2(y)\mathrm{d}y\\&-\int_0^1\eta_B'(y)\phi_1(y)\phi_0'(y)\phi_0(y)\mathrm{d}y-\int_0^1\eta_B(y)\eta_B''(y)\phi_0^3(y)\mathrm{d}y\\&+\int_0^1\eta_B'(y)\phi_0''(y)\phi_0^2(y)\mathrm{d}y\\&-\int_0^1\eta_B'(y)[\phi_0'(y)]^2\phi_0(y)\mathrm{d}y\Big\},\end{aligned}$$

$$I_3=\frac{1}{I}\Big[-\frac{3}{2}\int_0^1\eta_B''(y)\phi_2(y)\phi_0^2(y)\mathrm{d}y-\frac{1}{2c}\int_0^1\eta_B'''(y)\phi_0^4(y)\mathrm{d}y\Big],$$

$$I_4=\frac{c}{I}\int_0^1\phi_0^2(y)\mathrm{d}y.$$

Equation (23) delineates the propagation characteristics of Rossby wave amplitude within a fluid under air pressurization. This equation, known as the KdV–mKdV equation, has also been derived in various other contexts, including plasma physics. From a qualitative analytical perspective, the representation of I highlights that both the inclined topography and the β effect play pivotal roles in stimulating nonlinear Rossby waves. In summary, the influence of topography on the evolution of nonlinear Rossby waves, as captured by the present KdV–mKdV model equations, exhibits a complex nature, which is indispensable for our subsequent quantitative analysis.

3. Results

3.1. Introduction to numerical methods

In this section, we focus on conducting a quantitative analysis of the previously derived KdV–mKdV equation. To investigate the impact of nonlinear topography on the propagation of nonlinear Rossby solitary waves, we consider a sinusoidal topography given by $\eta_B(y)=B\sin\omega y$, where B and ω represent the amplitude and frequency of the topography, respectively, encapsulating the spatial characteristics of the terrain.

To delve deeper into the excitation, propagation, and dissipation of these nonlinear Rossby solitary waves, we must solve Eqs. (15), (18), and (19) to determine the coefficients appearing in Eq. (23). However, these equations constitute second-order Sturm–Liouville problems subject to fixed boundary conditions. According to the classical theory of Sturm–Liouville problems, finding analytical solutions to these equations is challenging. Consequently, the application of numerical methods becomes necessary to solve these equations effectively.

Self-adaptive loss-balanced physics-informed neural networks (lbPINNs)[38] are employed to solve the aforementioned equations. The basic principle of PINNs is to use neural network as a kind of function approximator to constrain the output of the network according to the physical model constraint, initial and boundary conditions of the equations known in advance, so as to obtain the solution of the equations following the physical laws. The framework of physics-informed neural networks is constructed in Fig. 1.

Without loss of generality, consider general nonlinear PDEs with the form

$$\begin{cases}u_t+\mathcal{N}_x[u,\eta]=0, x\in\Omega, t\in[0,T_0],\\u(x,0)=u_0(x,0), x\in\Omega,\\u(x,t)=u_0(x,t), x\in\partial\Omega, t\in[0,T_0],\end{cases} \quad (24)$$

where $x \in \Omega$ and $t \in [0, T_0]$ represent spatial and temporal coordinates. $\partial\Omega$ represents the boundary of the computational domain. The $\mathcal{N}_x$ represents the space-time differential operator parameterized by η. We seek solutions of the PDEs under the initial condition $u_0(x,0)$ and the boundary condition $u_0(x,t)$.

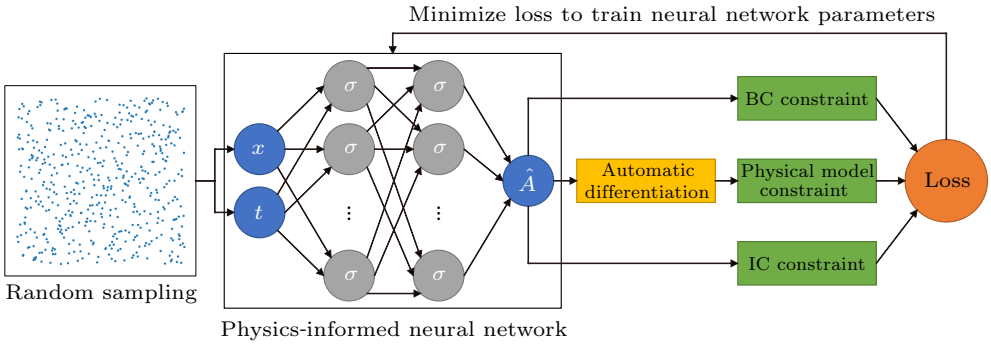


Fig. 1. The framework of the physics-informed neural networks (PINNs).

The neural network approximation $\hat{u}(x,t;\theta)$ solves $u(x,t)$ by optimizing parameters θ, where the loss function is formulated as

$$L(\theta;N) = \omega_u \cdot L_u(\theta;N_u) + \omega_r \cdot L_r(\theta;N_r), \tag{25}$$

where ω_u, ω_r are the loss weight parameters. L_u and L_r are defined as

$$\begin{cases} L_u(\theta;N_u) = \dfrac{1}{N_u}\displaystyle\sum_{j=1}^{N_u} \left| f\left(x_u^j, t_u^j; \theta\right)\right|^2, \\ L_r(\theta;N_r) = \dfrac{1}{N_r}\displaystyle\sum_{j=1}^{N_r} \left| \hat{u}\left(x_r^j, t_r^j; \theta\right) - u_0\left(x_r^j, t_r^j\right)\right|^2, \end{cases} \tag{26}$$

The first loss term L_u refers to the PDE residuals evaluated on randomly sampled localization points $\{x_u^j, t_u^j\}_{j=1}^{N_u}$ in the domain Ω. The second loss term L_r uses a set of training data $\{x_r^j, t_r^j\}_{j=1}^{N_r}$ to enforce the boundary and initial conditions.

With the idea of great likelihood, self-adaptive loss balanced PINNs points the weights are corrected to

$$L(\theta;N) = \frac{1}{2\varepsilon_u^2} \cdot L_u(\theta;N_u) + \frac{1}{2\varepsilon_u^2} \cdot L_r(\theta;N_r), \tag{27}$$

where ε_u, ε_r are trainable parameters, $\omega_u = 1/(2\varepsilon_u^2)$, $\omega_r = 1/(2\varepsilon_r^2)$ are adaptive weights.

3.2. Results analysis

Suppose that equation (23) has a solution of the form[39]

$$A(X,T) = N + M\mathrm{sech}^p(\xi), \tag{28}$$

where $\xi = k(X - vT - 2.5v)$, N, M, p, v are constants to be determined. Substituting Eq. (28) into Eq. (23), balancing $3p$ and $p+2$ thus $p = 1$, we have

$$\begin{cases} M = \sqrt{\dfrac{6I_4k^2}{I_3}}, \\ N = -\dfrac{I_2}{2I_3}, \\ v = I_2N + I_3N^2 + I_1 + I_4k^2. \end{cases} \tag{29}$$

Taking the parameters $c = 0.5$, $\omega = 0.5\pi$, $B = 1$, $\tilde{\beta} = 0.1$ as an example, we set the spatial domain $X \in \Omega = [-10, 10]$, the temporal domain $t \in [0, T_0] = [0, 5]$, and we can get the initial conditions and the boundary conditions of the equations when $k = 1$

$$A_0(X,T) = \sqrt{\frac{6I_4}{I_3}}\mathrm{sech}(X - vT - 2.5v) - \frac{I_2}{2I_3}. \tag{30}$$

We construct a neural network with 4 hidden layers and 60 neurons per layer, use tanh as the activation function of the neural network, and initialize the weights of each layer of the neural network with Xavier initialization.[40]

In the training phase of the neural network, 3000 training data coordinates were randomly sampled inside the equations using the Latin hypercube sampling method, 200 training data coordinates were machine-sampled on each of the initial and boundary conditions, respectively, and the Adam algorithm was utilized to iterate the neural network for 3×10^4 times.

In the testing phase of the neural network, gridded sampling ($\Delta x = 0.002$ and $\Delta t = 0.005$) was performed to obtain test data coordinates. The predicted values of the solutions of the equations at these coordinates are calculated using the trained neural network and compared with the analytical solutions of the equations. The training results are shown in Fig. 2.

In Fig. 2, subfigures (a), (b), and (c) show the images of the loss functions L, trainable parameters ε, and adaptive weights ω with the number of iterations in the lbPINNs algorithm, respectively. The loss function L shows a decreasing trend with iterations. Subfigures (d), (e), and (f) show the analytical forward solution, PINN forward solution, and PINN absolute error heat map of the KdV–mKdV equation, respectively. A relative L_2 error of 7.95×10^{-3} is achieved in solving the KdV–mKdV equation, indicating that the lbPINNs algorithm captures the spatiotemporal dynamical behavior of the KdV–mKdV equation well. Figure 3 illustrates the propagation of Rossby solitary waves under the parameters $c = 0.5$, $\tilde{\beta} = 0.1$, $\omega = 0.5\pi$, $B = 1$, which reveals that the solitary wave progresses westward over time.

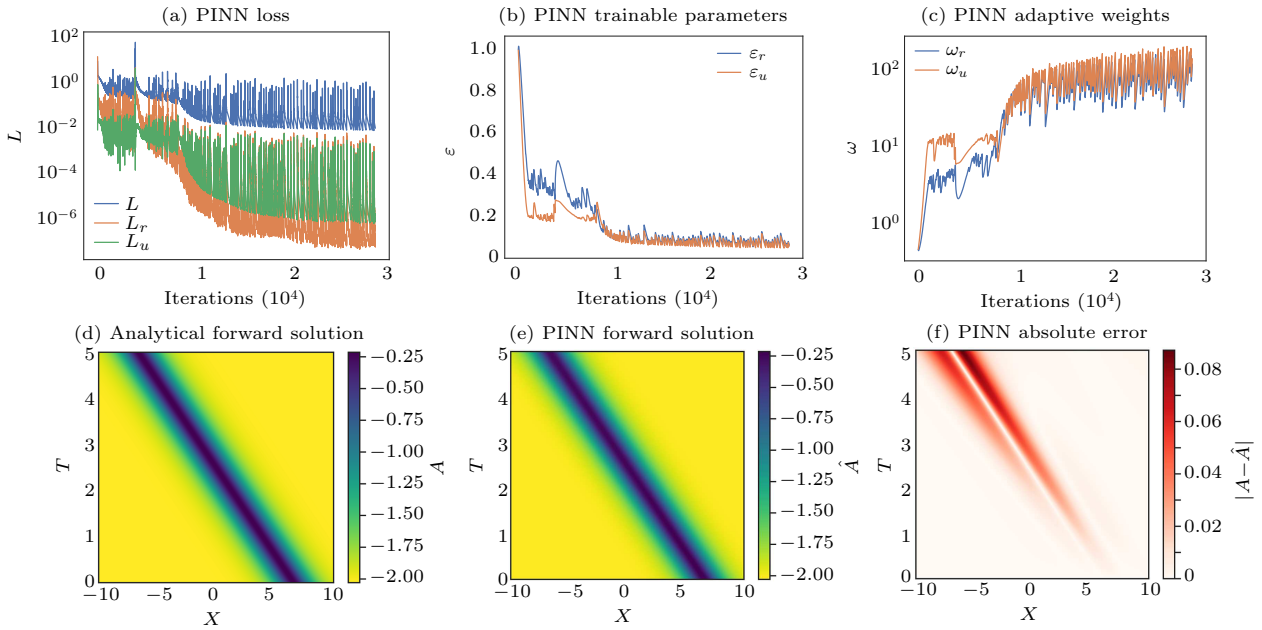


Fig. 2. The spatiotemporal dynamical behavior of the KdV–mKdV equation.

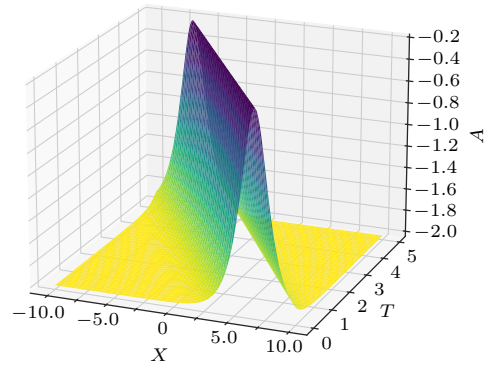


Fig. 3. Three-dimensional propagation images of the amplitude $A(X,T)$ of Rossby solitary wave with time T and space X at $c=0.5$, $\tilde{\beta}=0.1$, $\omega=0.5\pi$, $B=1$.

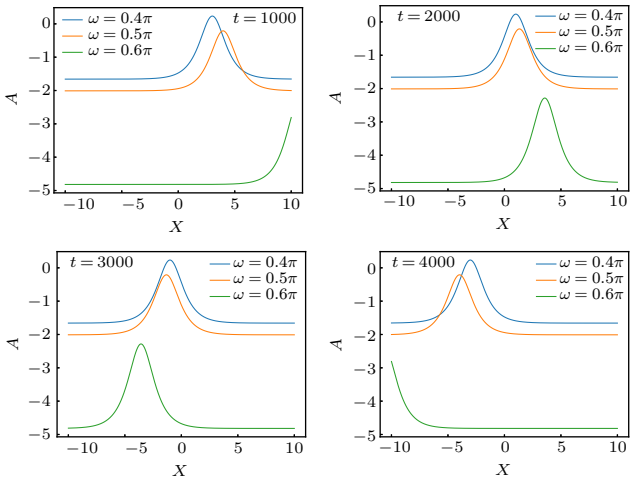


Fig. 4. Two-dimensional propagation images of the amplitude $A(X,T)$ of Rossby solitary wave with different angular velocities ω with $\delta=0.1$, $c=0.5$, $\tilde{\beta}=0.1$, $B=1$.

Figure 4 displays the propagation characteristic of a nonlinear Rossby solitary wave as it traverses bottom topography with varying frequencies ω. The findings indicate that as the frequency ω increases, the propagation speed of the Rossby wave also intensifies, while simultaneously, the interface of the Rossby wave descends. Conversely, the influence of frequency ω on the amplitude A of the Rossby wave remains relatively insignificant.

Figure 5 depicts the propagation characteristic of a nonlinear Rossby solitary wave as it traverses bottom topography with varying topographic amplitudes B. The results suggest that as the topographic amplitude B increases, the amplitude A of the Rossby wave decreases, while the velocity of the Rossby wave intensifies and its interface ascends.

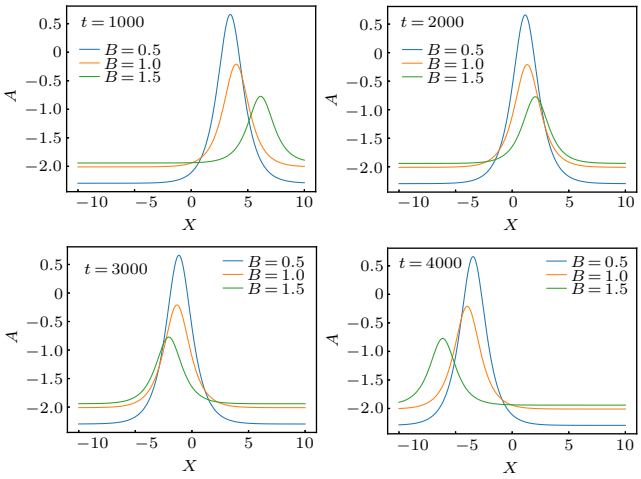


Fig. 5. Two-dimensional propagation images of the amplitude $A(X,T)$ of Rossby solitary wave with different angular velocities B with $\delta=0.1$, $c=0.5$, $\tilde{\beta}=0.1$, $\omega=0.5\pi$.

Figure 6 reveals the propagation characteristic of a nonlinear Rossby solitary wave as it traverses bottom topography with varying $\tilde{\beta}$. The evidence points to the fact that as $\tilde{\beta}$ increases, the interface of the Rossby wave ascends and its velocity decreases. Conversely, the amplitude A of the Rossby wave remains relatively unaffected by changes in $\tilde{\beta}$.

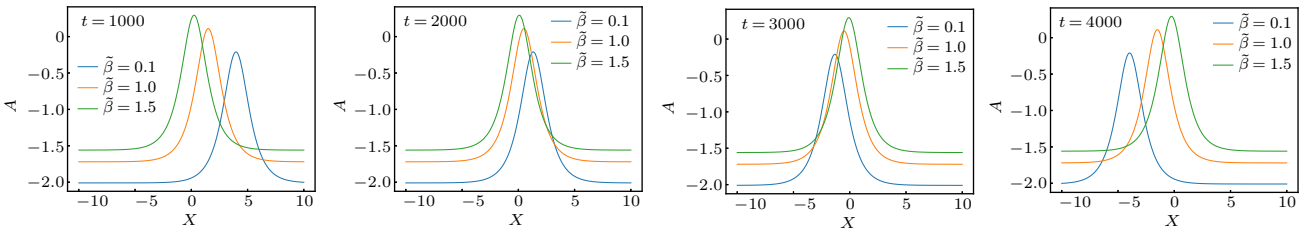


Fig. 6. Two-dimensional propagation images of the amplitude $A(X,T)$ of Rossby solitary wave with different angular velocities $\tilde{\beta}$ with $\delta = 0.1$, $c = 0.5$, $B = 1$, $\omega = 0.5\pi$.

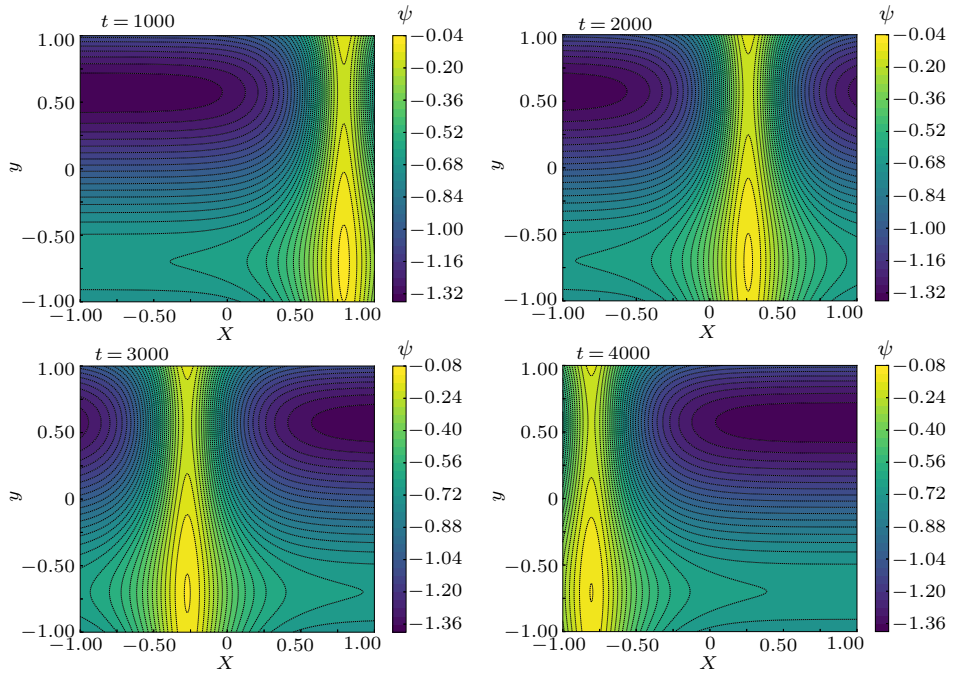


Fig. 7. The evolution of the stream field with $\delta = 0.1$, $c = 0.5$, $B = 1$, $\omega = 0.5\pi$, $\tilde{\beta} = 0.1$.

Figure 7 illustrates the evolution of the total stream field. The stream function ψ is approximated by the first and second terms of Eq. (12). Observing the contour plots of the stream function at moments t of 1000, 2000, 3000, and 4000, it can be seen that the stream function ψ exists as an isolated wave moving westward along the x-axis, i.e., propagating westward in the actual topography.

4. Conclusion

In this paper, we derived a KdV–mKdV model that captures the amplitude evolution of nonlinear Rossby waves from shallow water models incorporating topography. This derivation is achieved by utilizing the multiple scaling method and variable separation method, while taking into account physical factors such as the topography effect and β effect. Subsequently, the model is solved numerically using PINNs. The results demonstrate that both the frequency and amplitude of the topography are crucial factors influencing the evolution of Rossby waves. Specifically, an increase in the topography amplitude diminishes the propagation of Rossby solitary waves. Furthermore, variations of β also impact the evolution of Rossby solitary waves, primarily through changes in wave speed and interface position.

Acknowledgements

Project supported by the National Natural Science Foundation of China (Grant Nos. 12462021, 12102205, and 12262025), the Central Guidance for Local Scientific and Technological Development Funding Projects (Grant No. 2024ZY0117), the Program for Young Talents of Science and Technology in Universities of Inner Mongolia Autonomous Region (Grant No. NJYT23098), the Scientific Starting and the Innovative Research Team in the Universities of Inner Mongolia Autonomous Region of China (Grant No. NMGIRT2208), and the National College Students Innovation and Entrepreneurship Training Program (Grant No. 202410126024).

References

[1] Quartly G D, Cipollini P, Cromwell D and Challenor P G 2003 *Philos. Trans. A Math. Phys. Eng. Sci.* **361** 57
[2] Long R R 1964 *J. Atmos. Sci.* **21** 197
[3] Wadati M 1973 *J. Phys. Soc. Jpn.* **34** 1289
[4] Luo D 1997 *Dyn. Atmos. Oceans* **26** 53
[5] Ono H 1975 *J. Phys. Soc. Jpn.* **39** 1082

[6] Gottwald G A 2003 arXiv: nlin/0312009 [nlin.PS]
[7] Zhang H, Li B, Chen Y and Huang F 2010 *Chin. Phys. B* **19** 020201
[8] Hou S, Zhang R, Zhang Z and Yang L 2023 *Wave Motion* **124** 103249
[9] Yang X Q, *et al*. 2022 *Chin. Phys. B* **31** 070202
[10] Hodyss D and Nathan T R 2002 *Geophys. Astrophys. Fluid Dyn.* **96** 239
[11] Hodyss D and Nathan T R 2004 *Geophys. Astrophys. Fluid Dyn.* **98** 175
[12] Hodyss D and Nathan T R 2004 *J. Atmos. Sci.* **61** 2616
[13] Hodyss D and Nathan T R 2004 *Phys. Rev. Lett.* **93** 074502
[14] Charney J G and DeVore J G 1979 *J. Atmos. Sci.* **36** 1205
[15] Charney J G and Straus D M 1980 *J. Atmos. Sci.* **37** 1157
[16] Yang L, Da C, Song J, Zhang H, Yang H and Hou Y 2008 *Chin. J. Oceanol. Limnol.* **26** 334
[17] Zhang R, Yang L, Song J and Liu Q 2017 *Nonlinear Dyn.* **90** 815
[18] Zhang R, Yang L, Liu Q and Yin X 2019 *Appl. Math. Comput.* **346** 666
[19] Han F, Liu Q, Yin X and Zhang R 2024 *Phys. Fluids* **36** 1994
[20] Zhang Z, Zhang R, Wang J and Yang L 2023 *Nonlinear Dyn.* **111** 17483
[21] Song J, Yang L, Da C and Zhang H 2009 *Atmos. Ocean. Sci. Lett.* **2** 18
[22] Zhao Q, Fu Z and Liu S 2001 *Adv. Atmos. Sci.* **18** 418
[23] Ma W 2021 *Partial Differ. Equ. Appl. Math.* **5** 100220
[24] Abdou M A and Elhanbaly A 2007 *Commun. Nonlinear Sci. Numer. Simul.* **12** 1229
[25] Rasin A G and Schiff J 2017 *J. Nonlinear Sci.* **27** 45
[26] Fries T P and Belytschko T 2010 *Int. J. Numer. Methods Eng.* **84** 253
[27] Lee H G and Lee J Y 2014 *Comput. Math. Appl.* **68** 174
[28] Li Q, Luo K H, Kang Q J, He Y L, Chen Q and Liu Q 2016 *Prog. Energy Combust. Sci.* **52** 62
[29] Raissi M, Perdikaris P and Karniadakis G E 2019 *J. Comput. Phys.* **378** 686
[30] Lu L, Jin P, Pang G, Zhang Z and Karniadakis G E 2021 *Nat. Mach. Intell.* **3** 218
[31] Qi K and Sun J 2024 *Comput. Fluids* **274** 106239
[32] Yang Z, Dong Y, Deng X and Zhang L 2022 *Conn. Sci.* **34** 2500
[33] Edmundo F Lavia, *et al*. 2023 *Chin. Phys. B* **32** 054301
[34] Beck A, Flad D and Munz C D 2019 *J. Comput. Phys.* **398** 108910
[35] Almajid M M and Abu-Al-Saud M O 2022 *J. Pet. Sci. Eng.* **208** 109205
[36] Shu R, Wu H, Gao Y, Xu F, Gou R, Xiong W and Huang X 2025 *Environ. Res. Lett.* **20** 044030
[37] Li Q R, *et al*. 2023 *Chin. Phys. B* **32** 124701
[38] Xiang Z, Peng W, Liu X and Yao W 2022 *Neurocomputing* **496** 11
[39] Wang G and Wazwaz A M 2022 *Chaos, Solitons and Fractals* **155** 111694
[40] Glorot X and Bengio Y 2010 *Proceedings of the* 13*rd International Conferenceon Artificial Intelligence and Statistics*, May 13–15, 2010, Sardinia, Italy, p. 249